Properties and structure of $N=Z$ nuclei within relativistic mean field theory*

GAO Yuan(高远)[1,2;1)] DONG Jian-Min(董建敏)[2] ZHANG Hong-Fei(张鸿飞)[2]
ZUO Wei(左维)[2,3] LI Jun-Qing(李君清)[2,3]

1 (Hangzhou Dianzi University, Hangzhou 310018, China)
2 (School of Nuclear Science and Technology, Lanzhou University, Lanzhou 730000, China)
3 (Institute of Modern Physics, Chinese Academy of Sciences, Lanzhou 730000, China)

Abstract The axially deformed relativistic mean field theory with the force NLSH has been performed in the blocked BCS approximation to investigate the properties and structure of N=Z nuclei from Z=20 to Z=48. Some ground state quantities such as binding energies, quadrupole deformations, one/two-nucleon separation energies, root-mean-square (rms) radii of charge and neutron, and shell gaps have been calculated. The results suggest that large deformations can be found in medium-heavy nuclei with N=Z=38—42. The charge and neutron rms radii increase rapidly beyond the magic number N=Z=28 until Z=42 with increasing nucleon number, which is similar to isotope shift, yet beyond Z=42, they decrease dramatically as the structure changes greatly from Z=42 to Z=43. The evolution of shell gaps with proton number Z can be clearly observed. Besides the appearance of possible new shell closures, some conventional shell closures have been found to disappear in some region. In addition, we found that the Coulomb interaction is not strong enough to breakdown the shell structure of protons in the current region.

Key words mean field theory, BCS approximation,binding energy

PACS 21.10.Pc, 21.10.Dr, 21.60.-n

1 Introduction

The properties and structure of nuclei with equal numbers of protons and neutrons are receiving much attention at present. The structure of these nuclei provides useful information for isospin symmetry of nuclear force as well as shape coexistence[1—10]. Shape coexistence exists in a lot of N=Z nuclei, which means the prolate and the oblate (sometimes spherical shape) differ in the total energy only by several hundreds keV. These N=Z nuclei become proton-rich when the mass number reaches $A\sim 60$ and is close to the proton drip line with increasing mass number. The opportunities provided by the radioactive beam facilities make the investigation of the structure and properties of nuclei close to the proton drip line a very interesting and significant topic from both experimental and theoretical points of view. In the present work, the properties and structure of N=Z nuclei from Z=20 to Z=48 will be studied in the framework of axially deformed relativistic mean field (RMF) theory with the parameter set NLSH[11] in the blocked BCS approximation.

The RMF theory that automatically includes the spin-orbit interaction has been proven to be a powerful tool to describe and predict the properties of nuclei at the β-stable line as well as nuclei far from the β-stable line and superheavy nuclei[12—19]. It is well known that the BCS description of the scattering of nucleonic pairs from bound states to continuum states produces an unphysical procedure, which is obvious in neutron-rich nuclei. However, unlike the situation near the neutron drip line, for a proton-rich neutron the Coulomb barrier confines the protons in the interior of the nucleus. As a consequence, the effect of the coupling on the continuum is weaker and

Received 1 February 2009

* Supported by Natural Science Foundation of China (10775061, 10505016, 10575119), Fundamental Research Fund for Physics and Mathematics of Lanzhou University (LZULL200805), CAS Knowledge Innovation Project (KJCX-SYW-N02) and Major State Basic Research Developing Program of China (2007CB815004)

1) E-mail: gaoyuan@impcas.ac.cn

©2009 Chinese Physical Society and the Institute of High Energy Physics of the Chinese Academy of Sciences and the Institute of Modern Physics of the Chinese Academy of Sciences and IOP Publishing Ltd

therefore for nuclei close to the proton drip line, the RMF+BCS model could still be considered as a reasonable approximation providing sufficiently accurate results.

2 Theoretical background

The RMF theory is well known and will not be described in detail here. The interacting Lagrangian density is given by[20]:

$$\begin{aligned} L = & \overline{\psi}(\mathrm{i}\gamma^{\mu}\partial_{\mu}-M)\psi+\frac{1}{2}\partial_{\mu}\sigma\partial^{\mu}\sigma- \\ & \left(\frac{1}{2}m_{\sigma}^{2}\sigma^{2}+\frac{1}{3}g_{2}\sigma^{3}+\frac{1}{4}g_{3}\sigma^{4}\right)-g_{\sigma}\overline{\psi}\psi\sigma- \\ & \frac{1}{4}\Omega_{\mu\nu}\Omega^{\mu\nu}+\frac{1}{2}m_{\omega}^{2}\omega_{\mu}\omega^{\mu}-g_{\omega}\overline{\psi}\gamma^{\mu}\psi\omega_{\mu}- \\ & \frac{1}{4}R_{\mu\nu}R^{\mu\nu}+\frac{1}{2}m_{\rho}^{2}\rho_{\mu}\rho^{\mu}-g_{\rho}\overline{\psi}\gamma^{\mu}\tau\psi\rho- \\ & \frac{1}{4}F_{\mu\nu}F^{\mu\nu}-e\overline{\psi}\gamma^{\mu}\frac{1+\tau_{3}}{2}\psi A_{\mu}\,. \end{aligned}$$

The Dirac spinor ψ denotes the nucleon with the mass M. The quantities m_{σ}, m_{ω}, m_{ρ} are the masses of the σ, ω, ρ mesons respectively and the corresponding coupling constants are g_{σ}, g_{ω}, g_{ρ}. A_{μ} represents the photon field. The self-coupling terms with coupling constants g_2 and g_3 for the σ meson are introduced, which has turned out to be crucial[21]. The field tensors for the vector meson are given as $\Omega_{\mu\nu}=\partial_{\mu}\omega_{\nu}-\partial_{\nu}\omega_{\mu}$ and by similar expression for the ρ meson and the photon. One can obtain the Dirac equation for nucleons, Klein-Gordon equations for mesons and the Poisson equation for photons by varying the effective Lagrangian. The contributions of negative energy states are neglected (no-sea approximation). In the present work, the calculations are performed in the oscillator expansion method, which means that the bases of the Dirac equation and Klein-Gordon equations are taken as the eigenfunctions of the axially symmetric harmonic oscillator. The major shell is chosen as $Nf=14$ and $Nb=14$ for nucleons and mesons respectively. The paring correlations are accounted in the BCS formulism. For the strength of the pairing forces we have introduced the following forms for neutrons and protons, respectively[22]:

$$G_{\mathrm{n}}=\frac{21}{A}\left(1-\frac{N-Z}{2A}\right)\ \mathrm{MeV}, \tag{1}$$

$$G_{\mathrm{p}}=\frac{27}{A}\left(1+\frac{N-Z}{2A}\right)\ \mathrm{MeV}, \tag{2}$$

which depend on the proton number Z and neutron number N. In odd-A nuclei, the time reversal symmetry is broken. However, the effects of polarization currents and time-odd components in meson fields on the binding energy and deformation are very small and can be neglected to a good approximation[18, 22]. The blocking method is employed to deal with the unpaired nucleons, the state of which is chosen in such a way that the total single particle energy is a minimum[18, 22]. If the state of the last odd nucleon is k with energy ε_k, the total single-particle energy could be written as

$$E_{\mathrm{part}}=\varepsilon_k+2\sum_{i\neq k}\varepsilon_i v_i^2-\Delta\sum_{i\neq k}u_i v_i\,, \tag{3}$$

then the state k is determined by the variation of the total single-particle energy E_{part} with respect to k. Therefore, the Fermi energy, paring energy gap and E_{part} all depend on the choice of the unpaired odd nucleon state k.

3 Properties of $N=Z$ nuclei

The Fermi energies of the proton and neutron for N=Z nuclei have been shown in Fig. 1.

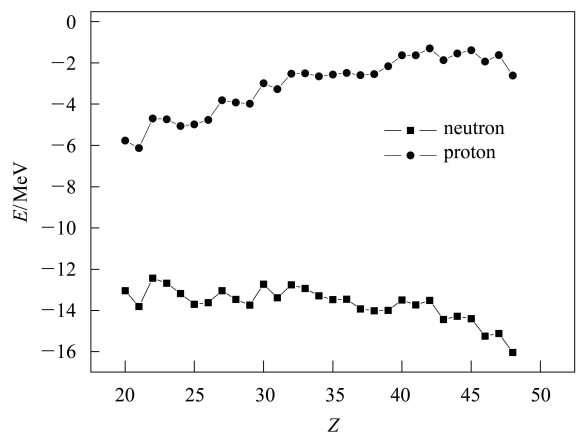

Fig. 1. The Fermi energy levels of the proton and neutron for N=Z nuclei.

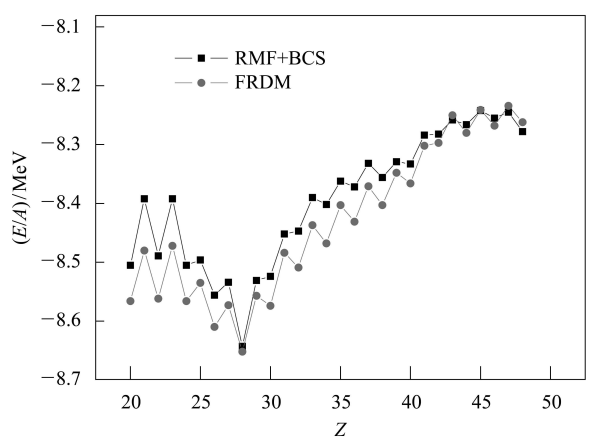

Fig. 2. The binding energy per nucleon for N=Z nuclei.

The neutron Fermi surface is very low and becomes lower with increasing proton number Z. The proton Fermi surface is much higher than that of the neutron due to proton-neutron interaction, and becomes higher with increasing Z. The highest proton Fermi energy is -1.2 MeV which indicates that the BCS approximation is still valid. For a given mass number A, the nucleus with the biggest absolute mean binding energy is most stable against β-decay, which can be taken as an approach to judge the stability of the nucleus. The binding energies per nucleon (B/A) for N=Z nuclei are shown in Fig. 2. The results from the finite-range droplet model (FRDM)[23, 24] are also presented for comparison. As can be seen, our calculated results are in good agreement with those from FRDM especially for larger Z nuclei, which differ from each other in the maximum absolute values by less than 1% in the current region. This suggests the RMF+BCS is reliable in this work. From the results of both theories, the minimum binding energy per nucleon locates at N=Z=28, because the neutron number Z=28 and the proton number N=28 are all magic numbers. The one-nucleon separation energy $S_{1\mathrm{n(p)}}$ and two-nucleon separation energy $S_{2\mathrm{n(p)}}$ are quite sensitive quantities to test a microscopic theory. The one-neutron/proton separation energy becomes negative when the nucleus is unstable against the one neutron/proton emission and similar for two-nucleon separation energy. The one-nucleon separation energies and two-nucleon separation energies for N=Z nuclei are plotted in Fig. 3 and Fig. 4 respectively. The one-nucleon separation energies fluctuate dramatically for the even-odd effect but there is no even-odd effect for two-nucleon separation energies. The neutron and proton shell closures at N=Z=28 can be clearly seen. The one/two-nucleon separation energies for nuclei with N=Z = 20—48 are all positive which indicates that these nuclei are all stable against one/two particle emission. No obvious evidence to indicate that N=Z=40 is a closure shell is seen, which agrees with what we discussed above and with other work[25]. The quadrupole deformation β_2 for N=Z nuclei is shown in Fig. 5.

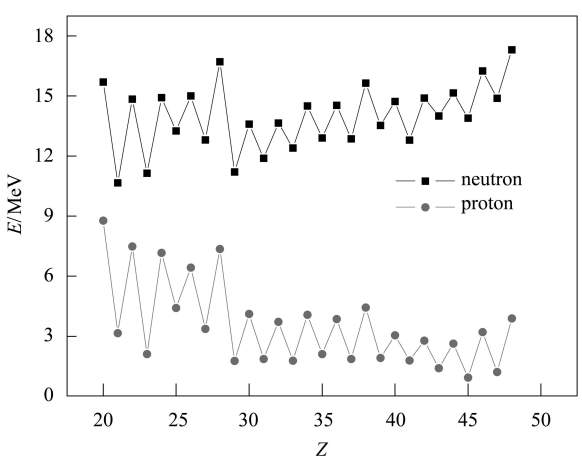

Fig. 3. One-nucleon separation energy for N=Z nuclei.

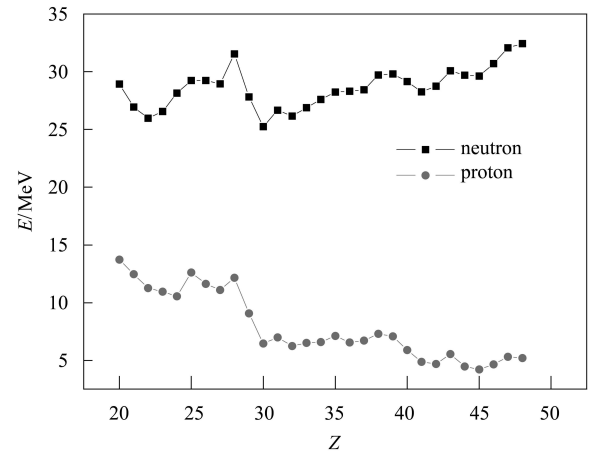

Fig. 4. Two-nucleon separation energy for N=Z nuclei.

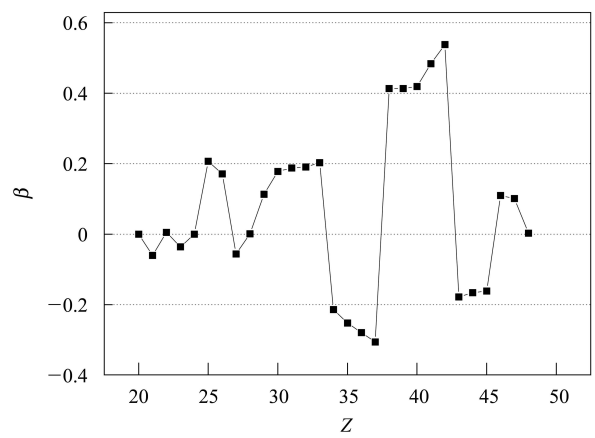

Fig. 5. The quadrupole deformation for N=Z nuclei.

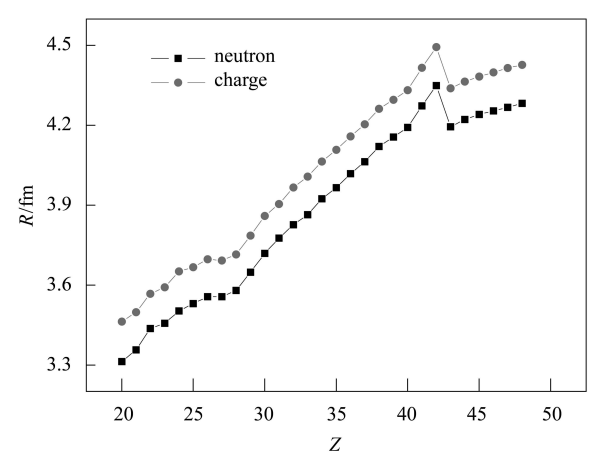

Fig. 6. The rms radii of charge and neutron for N=Z nuclei.

The prolate and oblate deformations appear alternately along with the increase of the proton number Z. One could notice that large deformations β_2=0.41—0.54 also exist in medium-heavy nuclei with Z=38—42. Because of deformation, the increased nuclear surface tension enhances the stability of the nucleus[26].

The rms radii of charge and neutron for N=Z nuclei obtained from RMF+BCS are plotted as a function of proton number Z in Fig. 6. The rms radius of charge is larger than that of the neutron due to Coulomb interaction between protons, and the rms radius difference $\Delta R = R_{\rm p} - R_{\rm n}$ increases by virtue of Coulomb interaction and gets stronger with increasing Z. With increasing proton number Z, the charge and neutron rms radii change slightly until they reach the magic number N=Z=28. Beyond this magic number, they increase rapidly with Z until they reach Z=42. This phenomenon results from the closure shell N=Z=28, which is similar to isotope shift. However, beyond Z=42, both charge and neutron rms radii decrease dramatically from Z=42 to Z=43, and then increase slightly. This could be traced back to the great nuclear structure change from Z=42 to Z=43, which corresponds to the great quadrupole deformation change from Z=42 to Z=43 as can be seen in Fig. 5. The changes of nuclear shape from large prolate (Z=42) to large oblate deformations (Z=43) lead to a great difference in nucleon distributions, and therefore rms radii change greatly.

4 Structure of $N=Z$ nuclei

The single-particle spectra of N=Z nuclei can be obtained in the deformed RMF+BCS calculation with the parameter set NLSH. The shell gaps at $Z(N)$=8, 10, 14, 16, 18, 20, 28, 38, 40, 50 are plotted as a function of proton number Z in Fig. 7. One could find that the shell gaps evolve with increasing Z. These denote that apart from the appearance of possible new shell closures at $Z(N)$=10, 14, 16 and 18, the conventional shell closures $Z(N)$=8, 20, 28 are found to disappear in some region. $N(Z)$=40 is only a small gap about 3.4 MeV for ^{80}Sr.

Figure 7 shows that the shell gaps are nearly identical for protons and neutrons, which indicates that the Coulomb interaction among protons is not too strong to breakdown the proton shell structure. Our calculations show that shape coexistence could be observed in many N=Z nuclei. The fact that a prolate and oblate shape coexistence exists at ^{84}Mo is obvious; its quadrupole deformations are -0.17 and 0.54 respectively, and the energy difference between the two configurations is 0.2 MeV. The density distributions of protons and neutrons along the z axis and $r_\perp$ axis are shown in Fig. 8 for ^{84}Mo with quadrupole

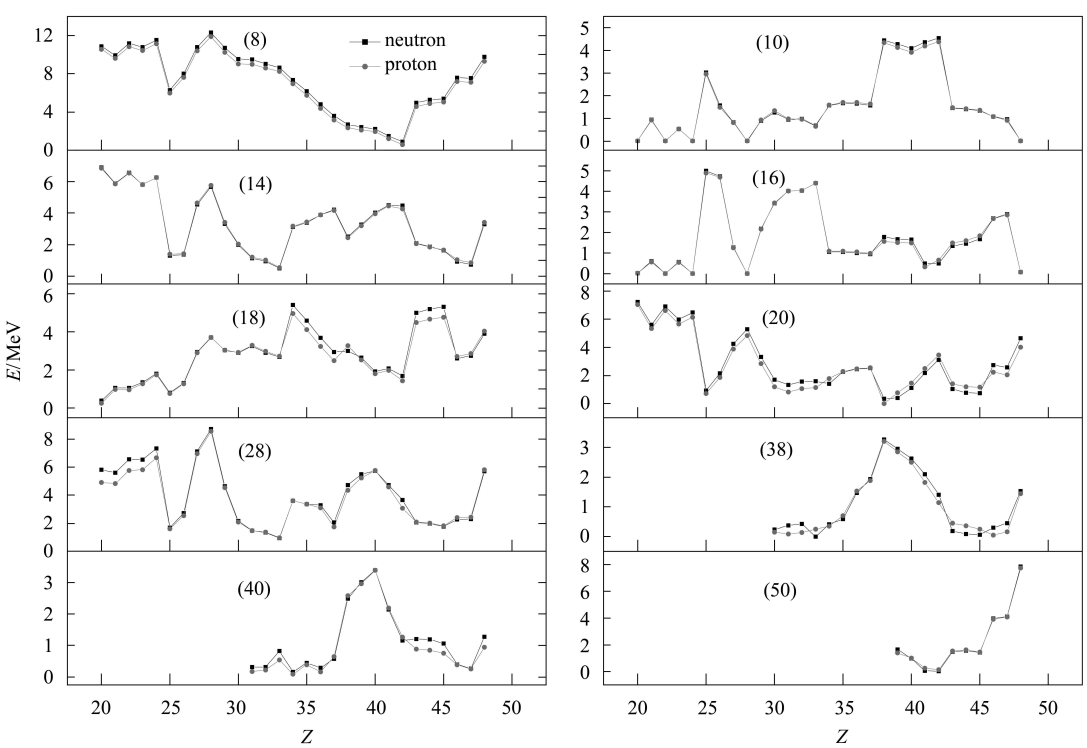

Fig. 7. The evolution of shell gaps with proton number Z for N=Z nuclei.

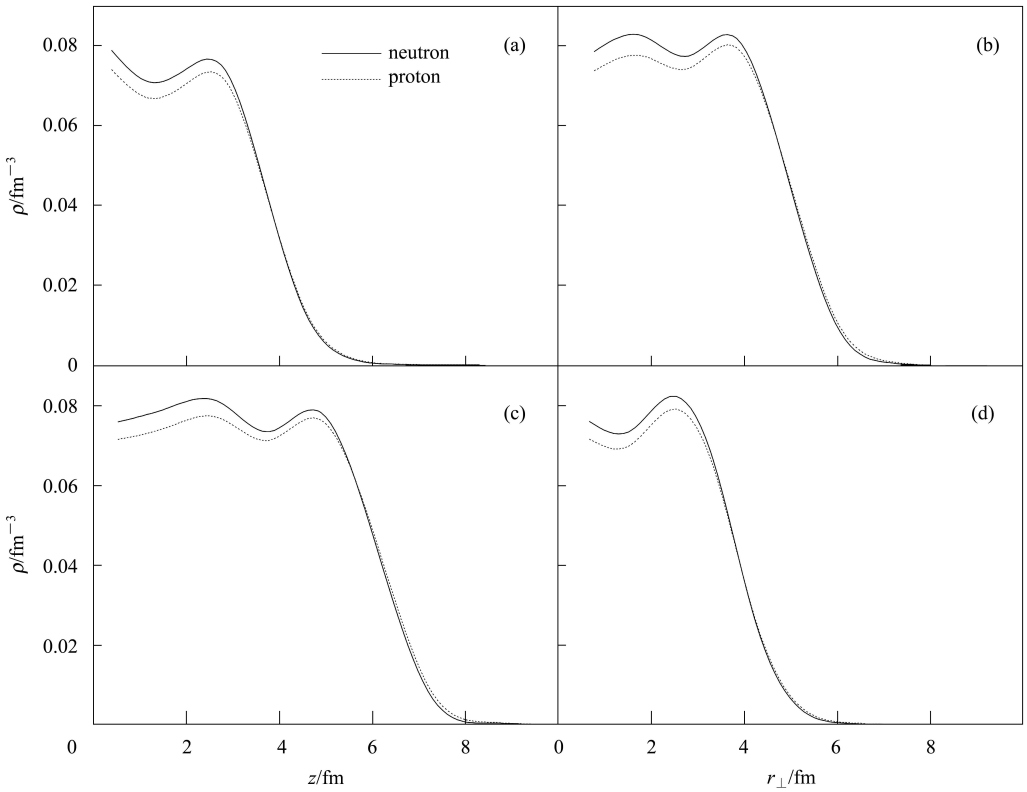

Fig. 8. The proton and neutron density distribution for ^{84}Mo with $\beta_2=-0.17$ (up) and 0.54 (down) along the z axis (left) and $r_\perp$ axis (right).

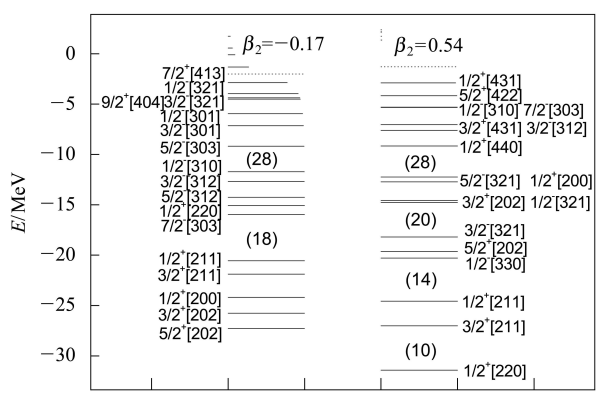

Fig. 9. The proton single-particle spectra of ^{84}Mo under shape coexistence (β_2=−0.17 and β_2=0.54).

deformations $\beta_2=-0.17$ and 0.54. A great difference in the density distributions between these two shapes could be found. In the interior of the nucleus, the proton density is slightly smaller than that of neutrons due to Coulomb interaction between protons and is slightly larger at the edge of the nucleus. The proton and neutron single-particle spectra for these two shape of ^{84}Mo are presented in Fig. 9 and Fig. 10. As can be seen, for a given shape ($\beta_2=-0.17$ or 0.54), the neutron and proton have nearly the same single-particle energy level sequence and distinct shell gaps appear at Z=N=18, 28 for $\beta_2=-0.17$ and Z=N=10, 14, 20, 28 for $\beta_2=0.54$. For a given particle (proton or neutron), the single-particle spectra are quite different, not only for shell gaps but also for the energy level sequence. The nucleus ^{84}Mo with the quadrupole deformation $\beta_2=0.54$ is more stable as the probability of nucleon distribution at positive levels is much smaller than that with $\beta_2=-0.17$. Though the nuclei have the nearly the same energy for different shapes when shape coexistence occurs, they have quite different structures.

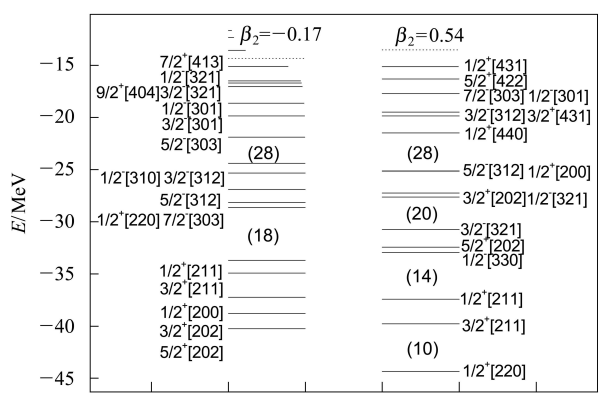

Fig. 10. The neutron single-particle spectra of ^{84}Mo under shape coexistence (β_2=−0.17 and β_2=0.54).

5 Summary and conclusions

The properties and structure of N=Z nuclei have been studied. Calculations have been performed in the axially deformed RMF with parameter set NLSH in the blocked BCS approximation. The binding energies, one/two-nucleon separation energies, proton and neutron rms radii, shell gaps and single-particle spectra have been obtained. The fact that the mean binding energies from RMF+BCS are in good agreement with those from FRDM connecting with low Fermi surface of protons demonstrates the validity of RMF+BCS in this work.

The results of one/two-nucleon separation energies indicate that N=Z=28 is a closed shell while N=Z=40 is not. Large deformations appear in medium-heavy nuclei for Z=38—42 with quadrupole deformations β_2=0.41—0.54. The charge and neutron rms radii increase rapidly beyond the magic number N=Z=28 until Z=42 with increasing proton number Z, which is similar to isotope shift. However, beyond Z=42, both charge and neutron rms radii decrease dramatically because the structure changes dramatically from Z=42 to Z=43 and corresponds to the quadrupole deformation change from 0.54(Z=42) to -0.18(Z=43). We also notice that the shell gap evolves with Z. The conventional shell closures at $Z(N)$=8, 20 and 28 disappear in a certain region and possible new shell closures appear at $Z(N)$=10, 14, 16 and 18. Shape coexistence exists in a lot of N=Z nuclei and the structure of different shapes under shape coexistence including single-particle spectra and shell structure is very different from each other. In addition, the Coulomb interaction is not strong to break down the proton shell structure. That is to say, protons and neutrons have nearly identical shell structure and shell gaps.

References

1 Heisenberg W. Z. Phys., 1932, **77**: 1
2 Lisetskiy A F et al. Phys. Phys. C, 1999, **60**: 064310—064316
3 Yamagami M, Matsuyanagi K, Matsuo M. Nucl. Phys. A, 2001, **693**: 579—602
4 Brentano P V et al. Nucl. Phys. A, 2002, **704**: 115—123
5 Petrovici A. Nucl. Phys. A, 2002, **704**: 144—153
6 Patra S K et al. Phys. Phys. C, 2002, **65**: 054323—054329
7 Kelsall N S et al. Phys. Phys. C, 2002, **65**: 044331—044343
8 Jenkins D G et al. Phys. Phys. C, 2002, **65**: 064307—064322
9 Petrovici A, Schmid K W, Faessler A. Nucl. Phys. A, 2002, **708**: 190—204
10 Regan P H et al. Nucl. Phys. A, 2007, **787**: 491—498
11 Sharma M M, Nagarajian M A, Ring P. Phys. Lett. B, 1993, **312**: 377—381
12 Vretenar D, Afanasjev A V, Lalazissis G A, Ring P. Phys. Rep., 2005, **409**: 101—259
13 MENG J et al. Prog. Part. Nucl. Phys., 2006, **57**: 470—563
14 Gangopadhyay G. Phys. Rev. C, 1999, **59**: 2541—2545
15 Sharma M M et al. Phys. Rev. Lett., 1994, **72**: 1431—1434
16 MENG J, Ring P. Phys. Rev. Lett., 1996, **77**: 3963—3966
17 REN Zhong-Zhou et al. Phys. Rev. C, 2002, **65**: 051304—051308
18 ZHANG Hong-Fei et al. Phys. Rev. C, 2005, **71**: 054312—054316
19 ZHANG Hong-Fei et al. Eur. Phys. J. A, 2006, **30**: 519—529
20 Gambhir Y K, Ring P, Thimet A. Ann. Phys., 1990, **198**: 132
21 Boguta J, Bodmer A R. Nucl. Phys. A, 1977, **292**: 413—428
22 LI Jun-Qing et al. Phys. Rev. C, 2002, **65**: 064305—064309
23 Möller P, Nix J R, Myers W D. At. Data Nucl. Data Tables, 1995, **59**: 185—381
24 Möller P, Nix J R, Kratz K L. At. Data Nucl. Data Tables, 1997, **66**: 131—343
25 Kanungo R. Phys. Lett. B, 2007, **649**: 31—34
26 Bohr A, Mottelson Ben R. Nuclear Structure II. New York: Benjamin, 1975. 605